

Atomically Dispersed Cobalt within a Bilayer of C₆₀Hualin Yang,[⊥] Ting Lai,[⊥] Haoxuan Ding,[⊥] Bosheng Li, Ying Gao, Jinbo Pan, Jianzhi Gao,* Shixuan Du,* Minghu Pan,* and Quanmin Guo*Cite This: *ACS Omega* 2025, 10, 10694–10700

Read Online

ACCESS |



Metrics & More

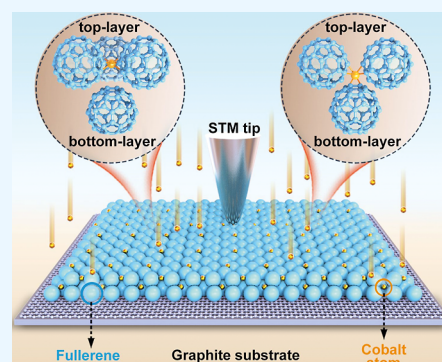


Article Recommendations



Supporting Information

ABSTRACT: Individual cobalt atoms trapped within a bilayer of C₆₀ have been produced by the deposition of Co atoms onto a C₆₀ double layer supported on graphite. High-resolution scanning tunneling microscopy (STM) reveals two stable states of a single cobalt atom coordinated with three C₆₀ molecules, which is denoted as (C₆₀)₃Co. The diffusion of the cobalt atoms within the C₆₀ layers is highly limited, resulting in the effective capture of single cobalt atoms in the interstitial sites of the close-packed C₆₀ layers. Density functional theory calculations show that the Co atom is located in the tetrahedral void between two close-packed C₆₀ layers. The most stable configuration of (C₆₀)₃Co consists of two C₆₀ molecules from the top layer with the third C₆₀ from the bottom layer. A less stable configuration of (C₆₀)₃Co where all three C₆₀ molecules are from the top layer was also observed at room temperature.



1. INTRODUCTION

The operation of a magnetic memory-storage device relies on the magnetic anisotropic energy of magnetic particles, which is predicted to be size-dependent at the atomic level and highly sensitive to the surrounding environment.¹ A single bit in a storage unit usually consists of millions of atoms. There is a strong demand in reducing the physical size of the bit toward the single molecule/atom level. Reading and writing with single-atom magnets have been demonstrated in the laboratory environment using scanning tunneling microscopy (STM), which probes and manipulates isolated holmium atoms supported by a magnesium oxide film.² Gambardella et al. have reported that single cobalt atoms exhibit giant magnetic anisotropy energy on the Pt(111) surface compared with the free atom due to symmetry reduction and the coordination with the substrate.³ However, it is a challenging task to create atomically dispersed materials due to the tendency of atoms to combine into clusters. If Co atoms are deposited directly onto a solid substrate such as graphite, the atoms tend to aggregate into large Co clusters.⁴ Such thermally controlled aggregation leads to a broad size distribution of the metal clusters.

Here, we report the trapping of individual cobalt atoms by two layers of C₆₀. We choose graphite-supported C₆₀ layers, which are known to be able to trap metal atoms by preventing the uncontrolled aggregation from taking place.⁵ We find that when a Co atom lands on top of the C₆₀ layers, it loses its mobility very quickly and becomes surrounded by three C₆₀ molecules. Density functional theory (DFT) calculations show that the trapped Co atom has a nonzero magnetic moment.⁶ If the temperature of the sample is sufficiently low, spontaneous polarization may order the magnetic moment. At room temperature (RT), we do not expect to observe a net

magnetization because thermal energy is well above magnetic energy. The focus of this work is on the physical process, which leads to the formation of (C₆₀)₃Co. The magnetic properties of the sample, such as its Curie temperature, are not measured.

The thermodynamic stability of the metal atom intercalated C₆₀ compound M_xC₆₀ has been analyzed by using the Born–Haber cycle theory.⁷ The results suggest that the transition metal (TM) intercalated C₆₀ compound may not be as stable as those formed with the alkali metals and early rare-earth. Nevertheless, the electron-donating property of the TM coupled with the substantial electron affinity of C₆₀ imply the possibility of forming stable TM_n-C₆₀ complexes.

Previous studies of the Co–C₆₀ mixed film by codepositing cobalt and C₆₀ have verified the formation of the Co–C₆₀ polymeric chain through the covalent bond.^{8–11} But these Co–C₆₀ polymeric chains are believed to be formed in a nonequilibrium state when codepositing cobalt and C₆₀ at RT. During the codeposition, the cobalt atoms and the C₆₀ molecules meet each other with great momentum, especially the C₆₀ molecules. Due to the relatively large size of C₆₀, the C₆₀ molecule has a great opportunity to meet several cobalt atoms during this process and form Co_n(C₆₀)_m complexes with different content ratios. By depositing individual Co atoms

Received: January 7, 2025

Revised: February 26, 2025

Accepted: March 3, 2025

Published: March 10, 2025



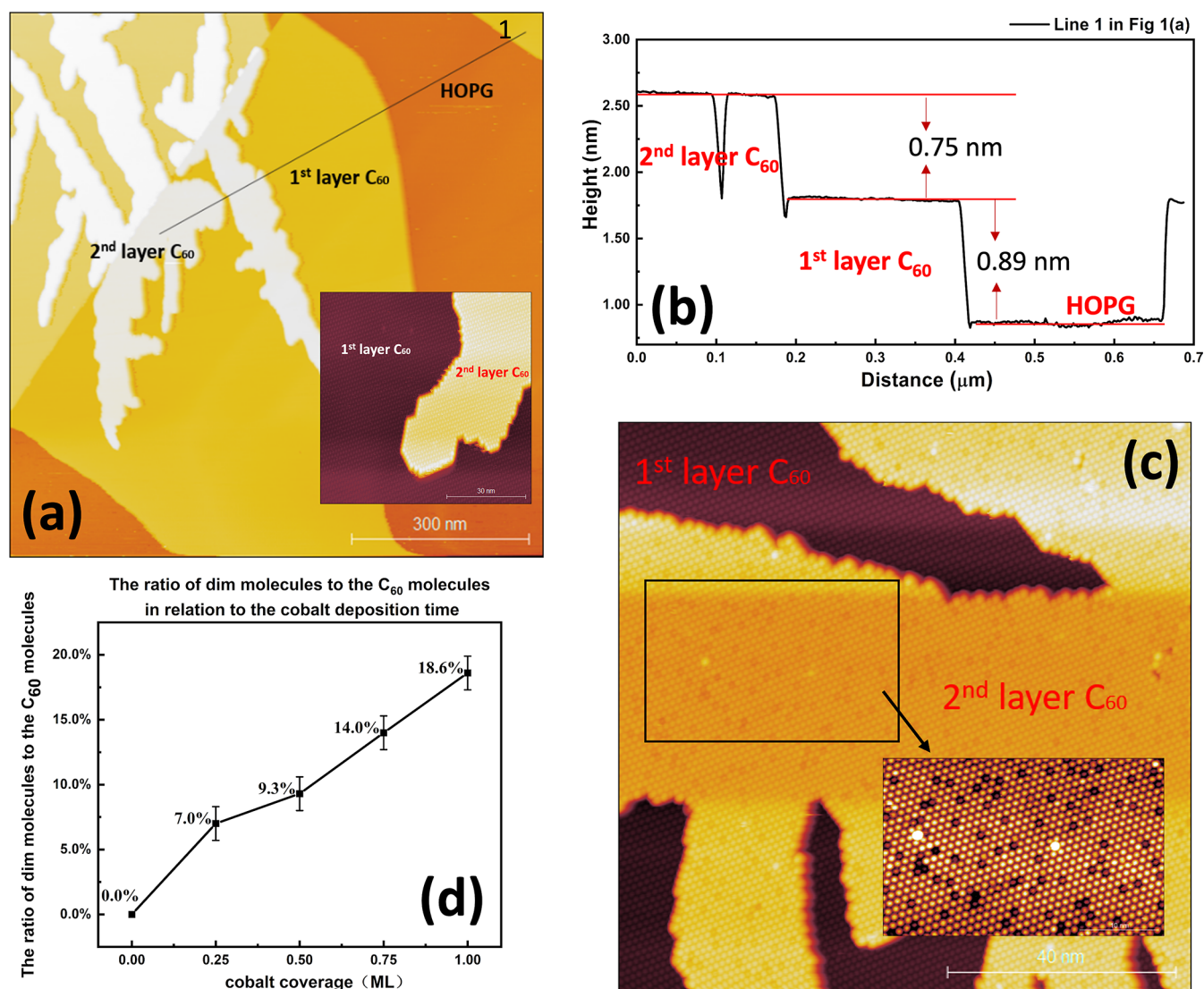


Figure 1. (a) Large-scale STM image of the bilayer C₆₀ molecules on HOPG. $I = 600$ pA, $V_{\text{bias}} = 1.8$ V. The inset is a local-scale STM image of bilayer C₆₀ molecules. $I = 600$ pA, $V_{\text{bias}} = 2.3$ V. (b) Height profile measured along line 1 in Figure 1a. The height of the first layer C₆₀ measured from the HOPG substrate is 0.89 nm; the second layer of C₆₀ is measured to be 0.75 nm taller than the first layer. (c) Large-scale STM image of the bilayer C₆₀ molecules after exposure to cobalt atoms. $I = 600$ pA, $V_{\text{bias}} = 1.8$ V. The inset is the local-scale STM image for the same area as marked by the rectangle in the large-scale STM image. $I = 600$ pA, $V_{\text{bias}} = 1.8$ V. (d) Percentage of dim molecules as a function of the cobalt coverage. The $\pm 1.3\%$ error includes variation in the number of dim molecules within 300 C₆₀ molecules from the different surface areas under each cobalt coverage. A ML of cobalt atoms on a close-packed C₆₀ layer is defined as the coverage where one cobalt atom exists in each unit cell of the close-packed C₆₀ lattice.

onto a preformed C₆₀ bilayer, we control the number of Co atoms in the Co_{*n*}(C₆₀)_{*m*} complexes to be one. STM images and DFT calculations suggest that (C₆₀)₃Co has formed involving C₆₀ molecules from both layers of the bilayer C₆₀ molecules.

2. RESULTS AND DISCUSSION

Monolayer (ML) and bilayer of C₆₀ were formed on highly oriented pyrolytic graphite (HOPG) by physical vapor deposition from a homemade Knudsen cell. Cobalt was deposited by using a CreaTec high-temperature effusion cell. All depositions were conducted with the HOPG sample at RT. C₆₀ molecules follow roughly a layer-by-layer growth mode with the second layer formed before the completion of the first layer. Figure 1a shows an STM image acquired after ~ 1 ML of C₆₀ has been deposited. The first layer of C₆₀ has smooth and rounded boundaries due to efficient edge diffusion. The second

layer of C₆₀ has a fractal-dendritic structure characteristic of kinetically controlled growth. This is due to a relatively high diffusion barrier arising from the corrugated potential energy surface presented by the first layer.¹² C₆₀ molecules within the same layer (first or second) appear at the same height as measured by STM. There are no molecules appearing "dim" or "bright" in the false-color image. It is known that C₆₀ molecules are free to rotate and flip at RT. Therefore, the molecules do not exhibit a fixed orientation,¹³ and STM images arise from a time-averaged signal for each molecule. The heights of the first and second layers of the C₆₀ islands on the HOPG substrate measured by STM are 0.89 and 0.75 nm, respectively, as shown in the height profile in Figure 1b.

Following the deposition of cobalt onto the preformed C₆₀ layers, we observed the appearance of "dim" C₆₀ molecules in the second layer, as shown in Figure 1c. The number of dim

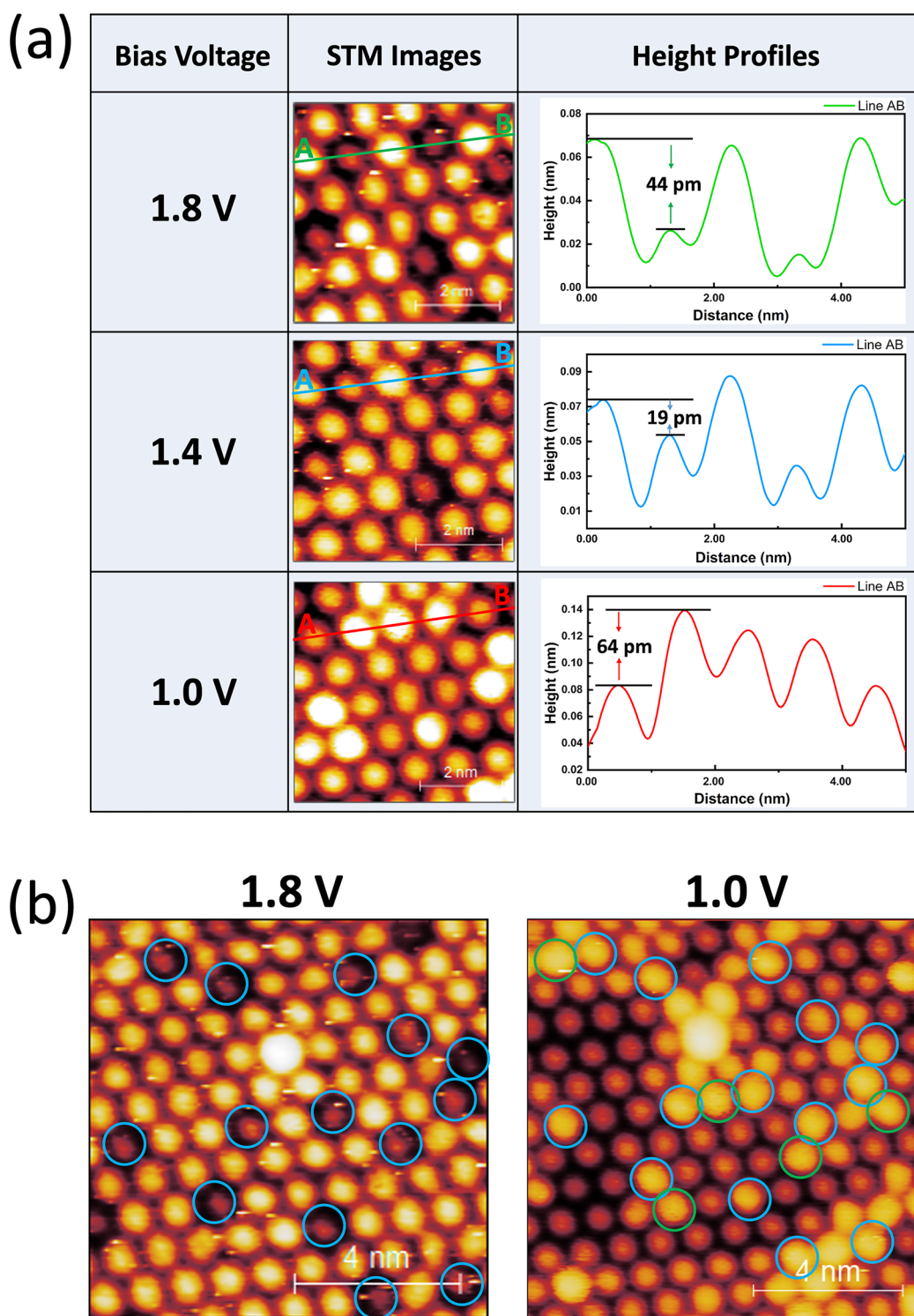


Figure 2. (a) STM images of the second layer of the bilayer C_{60} molecules after being exposed to the cobalt source for 3 min. The height profile was measured along line AB in the STM images with bias voltages of 1.8, 1.4, and 1.0 V, respectively. $I = 600$ pA, $V_{\text{bias}} = 1.8, 1.4$, or 1.0 V. (b) STM images with sample bias voltage of 1.8 and 1.0 V, respectively. The dark contrast in the STM image of 1.8 V corresponds to the bright contrast in the STM image of 1.0 V, as marked by blue circles. A few examples of C_{60} molecules with a bright contrast under 1.0 V but not showing dim under 1.8 V are marked by green circles. There is one extra bright C_{60} molecule in this image, and its brightness does not seem to depend on the bias voltage. It is possible that this extra bright molecule is sitting on a small Co cluster.

molecules increases linearly with the amount of cobalt deposited, as shown in Figure 1d. This is a direct piece of evidence that the dim C_{60} molecules are associated with deposited Co atoms. By counting the number of dim molecules and comparing with the number of Co atoms

delivered by the source, we find that roughly a single Co atom is linked to each dim C_{60} . The error involved in counting Co atoms arises mainly from the calibration of the Co evaporation source. It is known that Co can form a covalent bond with carbon in C_{60} .^{10,11} Hence, upon landing, a Co atom forms a

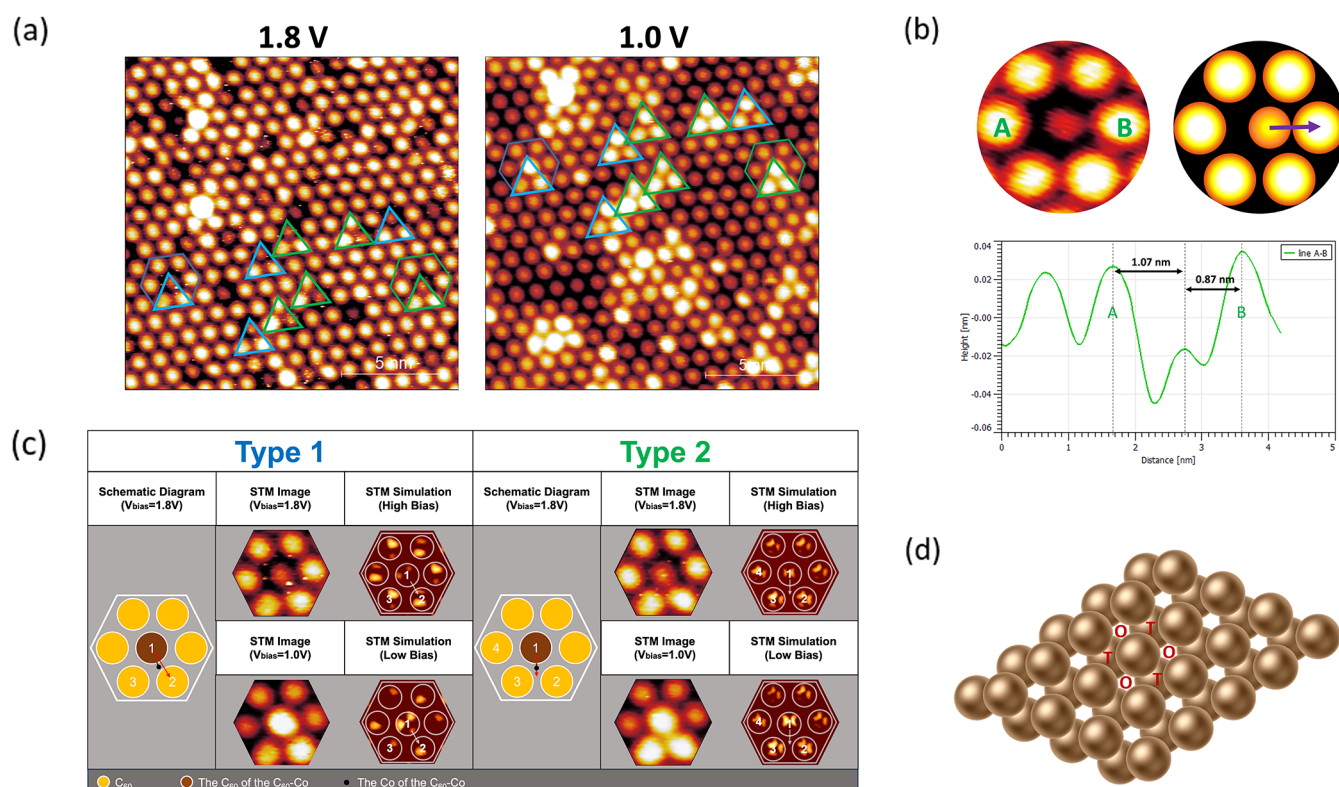


Figure 3. (a) STM images of the second layer of the bilayer C₆₀ after Co deposition. Left panel: $I = 600$ pA, $V_{\text{bias}} = 1.8$ V; right panel: $I = 600$ pA, $V_{\text{bias}} = 1.0$ V. The three C₆₀ molecules exhibit the features of type 1 or type 2 structures, which have been marked by blue and green triangles in the STM images, respectively. (b) STM image (left) and structural model (right) showing an apparent sideways displacement of the dim molecule. The height profile was measured along the line AB. $I = 600$ pA, $V_{\text{bias}} = 1.8$ V. (c) Comparison between observed STM images with those from DFT simulations. DFT refined structures can be found later in Figure 4. STM images acquired under 1.8 and 1.0 V are displayed. The simulated images were obtained under high-bias (1.30 eV above the Fermi level) and low-bias (0.83 eV above the Fermi level) conditions.

strong bond with a C₆₀ molecule and loses its mobility. This land and stick process prevents Co from forming Co clusters through lateral diffusion. There is a small fraction of dim molecules sitting next to each other due to two Co atoms landing on the surface ~ 1 nm apart.

The brightness contrast of these dim features is bias-dependent in the STM images. As shown in Figure 2a, the height profiles along line AB in the STM images were measured under three different bias voltages. Under 1.8 V sample bias, a dim C₆₀ molecule appears 44 pm lower than those in the immediate neighborhood. With a reduced bias of 1.4 V, the dim molecule appears 19 pm lower. For an even lower bias voltage of 1.0 V, the dim molecules observed with 1.8 and 1.4 V change into “bright” molecules, which appear 64 nm taller than those not showing bias-dependent contrast changes. Interestingly, it is not only the dim molecules at 1.8 V that have switched from dim to bright at 1.0 V, one or two molecules adjacent to each dim molecule also appear bright at 1.0 V, as shown in Figure 2b. Blue circles in Figure 2b mark the molecules that have gone through a dim to bright transition. Green circles mark the molecules that appear bright at 1.0 V, but not dim at 1.8 V.

The bias-dependent behavior of the C₆₀ molecules suggests that each Co atom is interacting with more than one C₆₀ molecule. The dim C₆₀ molecules in the STM image acquired at a 1.8 V bias voltage are probably the ones that are most strongly bound to Co. According to Raman spectra for the cobalt atom and the C₆₀ molecule mixed film, the C₆₀ molecules are negatively charged due to the charge transfer

from the cobalt atoms.⁸ This charge transfer makes the LUMO level of C₆₀ partially occupied.¹⁴ When the sample is biased at 1.4 V and above, the tunnel current is contributed by (i) direct tunneling from the STM tip to HOPG and (ii) tunneling via the LUMO of C₆₀. For a C₆₀ bonded with Co, its LUMO level is partly occupied by electrons, and hence, the LUMO becomes less effective in electron conduction when the sample is positively biased. This would make such a C₆₀ molecule appear dim in comparison to those not bonded with Co. When the bias voltage is reduced to below 1.0 V, the LUMO of C₆₀ is inaccessible.¹³ Tunneling current is then contributed solely from direct tunneling from tip to HOPG. However, since the tunnel gap is partly filled with C₆₀, the tunnel current is expected to remain dependent on C₆₀ via tip–molecule interactions. The formation of the Co–C₆₀ bond changes the way in which C₆₀ responds to the presence of the STM tip. While the usual interaction between the STM tip and C₆₀ is mainly of van der Waals (vdW) in nature, the formation of a Co–C₆₀ bond introduces an extra pathway of interaction due to the dipolar characteristics of the bond. When the tip is above a C₆₀ which is bonded to a Co atom, this molecule together with Co is subject to a stronger attractive interaction toward the tip. As a result, the molecule displaces upward and appears taller. In Figure 2b, it can be seen that under 1.0 V bias, a group of two or three C₆₀ molecules appear brighter than the surrounding molecules. This is an indication that a single Co atom interacts with two or three C₆₀ molecules from the top layer.

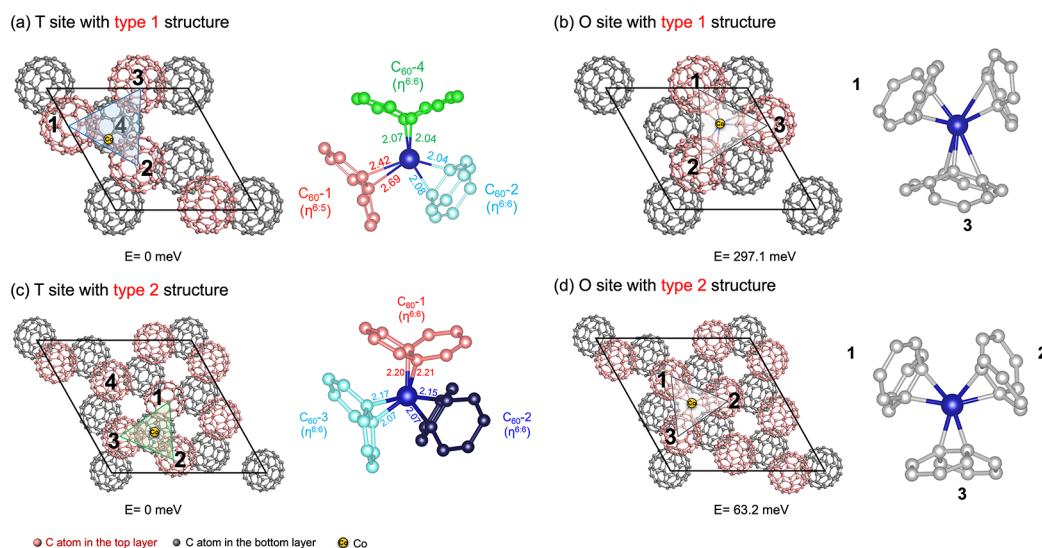


Figure 4. The relaxed structure models of cobalt atoms trapped in different interstitial sites of the C_{60} bilayer. (a,c) Configurations (left panels) and zoom-in bonding information around cobalt atoms (right panels) of type 1 and type 2 structures with cobalt atoms at the tetrahedral site (T site). (b,d) Configurations (left panels) and zoom-in bonding information around cobalt atoms (right panels) of type 1 and type 2 structures with cobalt atoms at the octahedral site (O site). The black parallelogram indicates a unit cell. The relative energy is presented at the bottom of each structure. The energy of the configuration with cobalt atom at T-site is taken as reference in both type of configurations.

A tentative explanation for the observed dim-bright contrast is given below. The STM feedback loop keeps the tunneling current at 600 pA during scanning by adjusting the distance between the tip and the sample surface. When the bias voltage is reduced from 1.8 to 1.0 V, the tip moves toward the surface. The reduced distance between the tip and sample results in a different electric field between the tip and surface molecules. In the regions of the C_{60} layer where no Co atoms are embedded, the interaction between the STM tip and the C_{60} molecule is relatively weak. In the cobalt-doped C_{60} regions, the bonding between the cobalt atom and the C_{60} molecule creates an electrical dipole, which is sensitive to the changing electrical field below the tip. The attraction from the tip can cause a significant upward displacement of the Co– C_{60} complex. As a result, under a 1.0 V bias voltage, the C_{60} molecules bonded with the cobalt atom appear bright. In Figure 3a, each blue triangle encloses a group of two bright C_{60} molecules at 1.0 V. This is qualitatively consistent with a bonding configuration where a Co atom bridges two C_{60} molecules in the top layer. We named this type of bonding type 1. Inside the green triangle, we see a group of three bright C_{60} molecules at 1.0 V. This is proposed as type 2 bonding where a Co atom is assumed to be linked to three C_{60} molecules from the top layer. For the sake of clarity of discussion, we label the relevant C_{60} molecules for each bonding type, as shown by the schematics in Figure 3c. In type 1 bonding, C_{60} -1 is the molecule that appears dim at 1.8 V. C_{60} -2 is the other molecule that appears bright at 1.0 V. In type 2 bonding, C_{60} -1 is the molecule that appears dim at 1.8 V. C_{60} -2 and C_{60} -3 are the other two molecules that appear bright at 1.0 V. In both cases, C_{60} -1 appears dim at 1.8 V but bright at 1.0 V.

In Figure 3c, we focus on the overall intensity and relative position associated with each C_{60} molecule. The intramolecular contrast from the STM simulation serves as a reference, which cannot be directly compared with STM data from the experiment due to the lack of resolution. (d) Structural model for the hexagonal closed-packed lattice of the bilayer C_{60} . The cobalt atom has the options of occupying the

tetrahedral site denoted as T or the octahedral site denoted as O.

We noticed that the dim C_{60} under 1.8 V shows a clear sideways shift in position. For type 1 bonding, the positional shift is toward C_{60} -2, as demonstrated in Figure 3b. This leads to a reduction of the distance between C_{60} -1 and C_{60} -2 from 1 to 0.87 nm. This reduction in the apparent distance is more likely due to a charge distribution change rather than a physical movement of C_{60} -1. For type 2 bonding, C_{60} -1 is observed to shift toward the midpoint between C_{60} -2 and C_{60} -3. For both types of bonding, C_{60} -1 shows no positional shift when imaged at 1.0 V. In Figure 3c, simulated STM images are shown, and they are in qualitative agreement with the experimental observations. Based on the tunneling current and bias voltage applied during scanning, it can be inferred that the scanning process involves a strong interaction between the tip and the sample. As a result, the position of C_{60} molecules that are weakly bonded to HOPG can be temporarily disturbed by the tip. However, these effects are not accounted for in the DFT simulation. The DFT simulation provides complementary information about the positions of the C_{60} molecules and their contribution to the tunneling current. The intramolecular structure revealed by DFT, however, is not directly comparable with experimental data. The simulated images are based on bonding configurations from DFT calculations, as shown in Figure 4.

For the double-layer C_{60} molecules, there are two kinds of interstitial sites, named the tetrahedral site (T site) and octahedral site (O site), as shown in Figure 3d. By comparing the DFT calculated relative energies shown at the bottom of Figure 4a,c for the type 1 bonding or at the bottom of Figure 4b,d for the type 2 bonding, Co tends to adsorb at the tetrahedral site rather than the octahedral site in both type 1 and type 2 bonding configurations, which agrees with the experiment that the blue and green triangles all have the same orientation, as depicted in Figure 3a. For type 1 bonding, the distance between C_{60} -1 and 2 is 9.875 Å, which is 0.354 Å shorter than the distance between C_{60} -1 and 3 in the Co-

deposited bilayer C_{60} crystal. In the left panel of Figure 4a, the C_{60} molecules labeled as 1, 2, and 3 come from the top layer, while the C_{60} molecule labeled as 4 comes from the bottom layer. The Co atom is bonded to C_{60} -1, 2, and 4 simultaneously. Although it appears that Co is bridging C_{60} -1 and 2, the bond lengths of Co with C_{60} -2 are shorter than those of Co with C_{60} -1, as shown in the right panel of Figure 4a. This difference indicates a stronger interaction of Co with C_{60} -2 compared with that of C_{60} -1. Consequently, the partial density of states for C_{60} -1 and 2 also shows a difference (Figure S1a). For type 2 bonding, as shown in Figure 4c, Co forms bonds with C_{60} -1, 2, and 3. All three molecules are from the top layer. Moreover, C_{60} -1 moves toward C_{60} -2 and 3 from its initial position by 0.474 Å. Shorter bond lengths of Co with C_{60} -2 and 3 than those of Co with C_{60} -1 are observed in the type 2 configuration (right panel of Figure 4c). A difference in partial density of states for C_{60} -1, 2, and 3 is displayed in Figure S1b.

The STM images give clear evidence of where the deposited Co atoms are and indications of how the atom is bonded to the C_{60} molecules. It is known that the tunnel current has contributions from topographical variations and density of state distributions. In addition, when imaging molecules, tip–molecule interaction introduces additional influences to the tunnel gap. STM images alone are not always sufficient to provide the information needed to determine the real space structure.¹⁵ When it comes to chemical bonding, there are a range of useful spectroscopic techniques such as XPS/UPS and ARPES that can provide valuable information in helping to determine how metal atoms are coordinated to organic molecules.¹⁶ By observing features around the Fermi level and core level shift, one can learn a lot about the direction of charge transfer. The STM itself when operating in its spectroscopic mode (STS) can also reveal the density of state information. The VT-STM used in this study can be cooled via a continuous flow of a cryogenic liquid. The flow of liquid makes it difficult to maintain a constant temperature because only the sample is cooled, not the tip. Attempts to collect STS data from this STM resulted in poor reproducibility. The DFT calculations give us some information about the C_{60} –cobalt bonding and the stability of the proposed structures. It is not possible to simulate under exactly the same conditions as those in the experiment. Some aspects of the STM imaging, such as tip–molecule interaction, are difficult to include in simulations. Nevertheless, DFT simulations have given useful guidelines when several possible structures are compared. The structure of $(C_{60})_3Co$, as determined by the STM experiment and DFT calculations, is in good agreement with the observation of $(C_{60})_3Co$ clusters in the gas phase.¹⁷

3. CONCLUSIONS

In summary, we have produced atomically dispersed cobalt embedded in a bilayer of C_{60} . Observations using STM in conjunction with DFT calculations reveal the formation of $(C_{60})_3Co$. There are two bonding configurations for $(C_{60})_3Co$, both involving cobalt located near the tetrahedral void provided by the C_{60} layers. In one bonding configuration, two molecules from the top layer and one from the bottom layer are bonded to cobalt. In the other configuration, cobalt is bonded to three C_{60} molecules, all from the top layer. C_{60} molecules bonded to cobalt show strong bias-dependent behavior, which arises from the nature of the C_{60} –Co bond.

4. METHODS

4.1. STM Experiments. All experiments were conducted in an ultrahigh-vacuum (UHV) chamber with a base pressure of 3.0×10^{-10} mbar. The STM imaging was performed using an Omicron VT-STM at RT. The electrochemically etched tungsten tip was used for the STM imaging. The HOPG used as the substrate is of ZYA grade. The HOPG was cleaved using scotch tape before being transferred into the UHV chamber. The HOPG was then annealed at 613 K for 1 h in the UHV chamber to remove surface contaminants. The C_{60} MLs and bilayers are prepared by thermally evaporating C_{60} powders (purity of 99%) from a homemade Knudsen cell onto the HOPG substrate at a rate of 0.1 ML min^{-1} for 10 min. The cobalt was deposited onto the substrate by using a CreaTec high-temperature effusion cell at a rate of $0.025 \text{ ML min}^{-1}$. All depositions were conducted with the HOPG substrate at RT and a background vacuum better than 3.0×10^{-9} mbar.

4.2. DFT Simulations. DFT calculations were performed using the Vienna ab initio simulation package.¹⁸ The projector-augmented wave potentials with the generalized gradient approximation of Perdew–Burke–Ernzerhof formulation was employed to treat the electron–ion interactions and exchange–correlation functions.^{19–21} To better describe the 3d electrons of TM elements, the DFT + U method proposed by Dudarev et al. with an effective U value of 3.0 eV was employed to the Co element.²² Grimme’s D3 correction was adopted to describe the vdW interaction.²³ The initial supercell contains two layers of C_{60} with one Co atom adsorbed. The neighboring C_{60} is separated by ~ 1 nm. For geometrical optimization, all of the atoms were fully relaxed to reach a force tolerance of 0.02 eV Å^{-1} . We employed a size of $\sqrt{3} \times \sqrt{3}$ and $\sqrt{7} \times \sqrt{7}$ supercell to represent type 1 and type 2 structures. A vacuum gap of $>13 \text{ Å}$ was added to prevent the interaction between slabs in each supercell. The cutoff energy was 600 eV (400 eV) in the $\sqrt{3} \times \sqrt{3}$ ($\sqrt{7} \times \sqrt{7}$) supercell, and the K-point mesh was gamma only. The partial charge densities were calculated to simulate the STM images according to the Tersoff–Hamann approach.²⁴

■ ASSOCIATED CONTENT

Data Availability Statement

All data are available within the manuscript.

Supporting Information


The Supporting Information is available free of charge at <https://pubs.acs.org/doi/10.1021/acsomega.5c00176>.


DFT simulation for the projected density of states of C_{60} in type 1 and type 2 configurations(PDF)

■ AUTHOR INFORMATION

Corresponding Authors

Jianzhi Gao – School of Physics and Information Technology, Shaanxi Normal University, Xian 710119, China; Email: jianzhigao@snnu.edu.cn

Shixuan Du – Institute of Physics, Chinese Academy of Science, Beijing 100190, China;  orcid.org/0000-0001-9323-1307; Email: sxdu@iphy.ac.cn

Minghu Pan – School of Physics and Information Technology, Shaanxi Normal University, Xian 710119, China;  orcid.org/0000-0002-1520-209X; Email: minghupan@snnu.edu.cn

Quanmin Guo – School of Physics and Astronomy, University of Birmingham, Birmingham B15 2TT, U.K.; orcid.org/0000-0002-3417-8726; Email: Q.GUO@bham.ac.uk

Authors

Hualin Yang – School of Physics and Astronomy, University of Birmingham, Birmingham B15 2TT, U.K.; orcid.org/0000-0003-1067-8643

Ting Lai – Institute of Physics, Chinese Academy of Science, Beijing 100190, China

Haoxuan Ding – School of Physics and Astronomy, University of Birmingham, Birmingham B15 2TT, U.K.; School of Materials Science and Engineering, Peking University, Beijing 100871, People's Republic of China

Bosheng Li – School of Physics and Astronomy, University of Birmingham, Birmingham B15 2TT, U.K.; orcid.org/0000-0002-8510-4006

Ying Gao – School of Physics and Astronomy, University of Birmingham, Birmingham B15 2TT, U.K.

Jinbo Pan – Institute of Physics, Chinese Academy of Science, Beijing 100190, China; orcid.org/0000-0003-2612-8232

Complete contact information is available at:

<https://pubs.acs.org/10.1021/acsomega.5c00176>

Author Contributions

¹H.Y., T.L., and H.D. contributed equally to this work. H.Y. initiated the project and conducted the experiments. T.L. and J.P. performed the DFT simulations. H.D., Y.G., B.L., J.G., S.D., M.P., and Q.G. contributed to data analysis and writing of the manuscript with inputs from all other authors.

Notes

The authors declare no competing financial interest.

ACKNOWLEDGMENTS

Sample growth and STM work was conducted at School of Physics and Astronomy, University of Birmingham, United Kingdom. This work was financially supported by the National Natural Science Foundation of China (No. 22372096).

REFERENCES

- (1) Oyarzún, S.; Tamion, A.; Tournus, F.; Dupuis, V.; Hillenkamp, M. Size Effects in the Magnetic Anisotropy of Embedded Cobalt Nanoparticles: from Shape to Surface. *Sci. Rep.* **2015**, *5*, 14749–14757.
- (2) Natterer, F. D.; Yang, K.; Paul, W.; Willke, P.; Choi, T.; Greber, T.; Heinrich, A. J.; Lutz, C. P. Reading and Writing Single-Atom Magnets. *Nature* **2017**, *543*, 226–228.
- (3) Gambardella, P.; Rusponi, S.; Veronese, M.; Dhesi, S. S.; Grazioli, C.; Dallmeyer, A.; Cabria, I.; Zeller, R.; Dederichs, P. H.; Kern, K.; et al. Giant Magnetic Anisotropy of Single Cobalt Atoms and Nanoparticles. *Science* **2003**, *300*, 1130–1133.
- (4) Wong, P. K. J.; de Jong, M. P.; Leonardus, L.; Siekman, M. H.; van der Wiel, W. G. Growth Mechanism and Interface Magnetic Properties of Co Nanostructures on Graphite. *Phys. Rev. B* **2011**, *84*, 054420–054426.
- (5) Guo, L. A.; Wang, Y.; Bao, D.-L.; Jia, H.-H.; Wang, Z.; Du, S.; Guo, Q. On-surface Synthesis of Size- and Shape-Controlled Two-dimensional Au_n Nanoclusters Using a Flexible Fullerene Molecular Template. *Nanoscale* **2020**, *12*, 21657–21664.
- (6) Chegeni, M. H.; Boostani-Poor, R.; Jalilian, J. Spin and Orbital Magnetism of Exohedral Fullerene Doped with Single Transition Metal Atom (Sc-Ni): A Relativistic Density Functional Theory Study. *Comput. Theor. Chem.* **2022**, *1215*, 113842–113850.
- (7) Tománek, D.; Wang, Y.; Ruoff, R. S. Stability of Fullerene-Based Systems. *J. Phys. Chem. Solids* **1993**, *54*, 1679–1684.
- (8) Lavrentiev, V.; Abe, H.; Yamamoto, S.; Naramoto, H.; Narumi, K. Isolation of Co Nanoparticles by C₆₀ Molecules in Co-Deposited Film. *Mater. Lett.* **2003**, *57*, 4093–4097.
- (9) Lavrentiev, V.; Abe, H.; Yamamoto, S.; Naramoto, H.; Narumi, K. Formation of Promising Co–C Nanocompositions. *Surf. Interface Anal.* **2003**, *35*, 36–39.
- (10) Sakai, S.; Naramoto, H.; Avramov, P. V.; Yaita, T.; Lavrentiev, V.; Narumi, K.; Baba, Y.; Maeda, Y. Comparative Study of Structures and Electrical Properties in Cobalt–Fullerene Mixtures by Systematic Change of Cobalt Content. *Thin Solid Films* **2007**, *515*, 7758–7764.
- (11) Sakai, S.; Yakushiji, K.; Mitani, S.; Sugai, I.; Takanashi, K.; Naramoto, H.; Avramov, P. V.; Lavrentiev, V.; Narumi, K.; Maeda, Y. Magnetic and Magnetotransport Properties in Nanogranular Co/C₆₀-Co Film with High Magnetoresistance. *Mater. Trans.* **2007**, *48*, 754–759.
- (12) Liu, H.; Reinke, P. C₆₀ Thin Film Growth on Graphite: Coexistence of Spherical and Fractal-Dendritic Islands. *J. Chem. Phys.* **2006**, *124*, 164707–164712.
- (13) Nakaya, M.; Kuwahara, Y.; Aono, M.; Nakayama, T. Reversibility-Controlled Single Molecular Level Chemical Reaction in a C₆₀ Monolayer via Ionization Induced by Scanning Transmission Microscopy. *Small* **2008**, *4*, 538–541.
- (14) Matsumoto, Y.; Sakai, S.; Naramoto, H.; Hirao, N.; Baba, Y.; Sugai, I.; Takanashi, K.; Shimada, T.; Maeda, Y. The Electronic Structures of Fullerene/Transition-Metal Hybrid Material. *MRS Online Proc. Libr.* **2008**, *1081*, 1081-P07-01.
- (15) Yamada, T. K.; Nemoto, R.; Nishino, F.; Hosokai, T.; Wang, C.-H.; Horie, M.; Hasegawa, Y.; Kera, S.; Krüger, P. On-Surface Growth of Transition-Metal Cobalt Nanoclusters Using a 2D Crown-Ether Array. *J. Mater. Chem. C* **2024**, *12*, 874–883.
- (16) Gottfried, J. M. Surface Chemistry of Porphyrins and Phthalocyanines. *Surf. Sci. Rep.* **2015**, *70*, 259–379.
- (17) Kurikawa, T.; Nagao, S.; Miyajima, K.; Nakajima, A.; Kaya, K. Formation of Cobalt–C₆₀ Clusters: Tricapped Co(C₆₀)₃ Unit. *J. Phys. Chem. A* **1998**, *102*, 1743–1747.
- (18) Vanderbilt, D. Soft Self-Consistent Pseudopotentials in a Generalized Eigenvalue Formalism. *Phys. Rev. B* **1990**, *41*, 7892–7895.
- (19) Kresse, G.; Joubert, D. From ultrasoft pseudopotentials to the projector augmented-wave method. *Phys. Rev. B* **1999**, *59*, 1758–1775.
- (20) Perdew, J. P.; Burke, K.; Ernzerhof, M. Generalized Gradient Approximation Made Simple. *Phys. Rev. Lett.* **1996**, *77*, 3865–3868.
- (21) Perdew, J. P.; Chevary, J. A.; Vosko, S. H.; Jackson, K. A.; Pederson, M. R.; Singh, D. J.; Fiolhais, C. Atoms, Molecules, Solids, and Surfaces: Applications of the Generalized Gradient Approximation for Exchange and Correlation. *Phys. Rev. B* **1992**, *46*, 6671–6687.
- (22) Dudarev, S. L.; Botton, G. A.; Savrasov, S. Y.; Humphreys, C. J.; Sutton, A. P. Electron-Energy-Loss Spectra and the Structural Stability of Nickel Oxide: An LSDA+U Study. *Phys. Rev. B* **1998**, *57*, 1505–1509.
- (23) Grimme, S.; Antony, J.; Ehrlich, S.; Krieg, H. A consistent and accurate ab initio parametrization of density functional dispersion correction (DFT-D) for the 94 elements H–Pu. *J. Chem. Phys.* **2010**, *132*, 154104–154123.
- (24) Tersoff, J.; Hamann, D. R. Theory of the Scanning Tunneling Microscope. *Phys. Rev. B* **1985**, *31*, 805–813.